



Figure 1. Contour plot of ratio of maximum shear stress to maximum Coulomb strength as a function of position around tip of a propagating right-lateral slip pulse for different inclination angles of the initial most compressive stress,  $Y = (1/2)\tan^{-1}[2s_{xy}^0/(s_{xx}^0 - s_{yy}^0)]$ , with the fault in a medium without and with undrained poroelastic response for (left) Skempton  $B = 0$  and (right)  $B = 0.6$ , respectively. The seismic  $S$  ratio is 6.4 and  $f_r/f_d = 0.2$ . Rupture speeds are scaled with the shear wave speed  $C_s$  (so that these cases are very near the Rayleigh wave speed,  $0.92C_s$ ), and distance with the scale length  $R_o^*$  (called  $R_o$  in the text) that the slip-weakening zone would have at very low propagation speed and under a prestress corresponding to a large value of the seismic  $S$  ratio. Adapted from Rice et al. [2005].

saturation of off-fault material. We present a linear poroelasto-plastic constitutive relationship for undrained behavior (i.e., stressing on a timescale much shorter than the timescale for fluid to leave the length scale of interest), based upon the constitutive relationship for drained behavior (i.e., no change in pore pressure, readily the case for “dry” materials) of part 1. Subsequently, we study how undrained behavior affects the distribution and magnitude of off-fault plastic deformation, the rupture dynamics, and the localized deformation.

## 2. Background and Theory

[5] We proceed in two stages in developing our fault model to be representative of saturated porous media. We first consider linear poroelastic behavior. We then go on to consider poroelastoplastic response, including the occurrence of plastic dilatancy, and the consequent feedback on pore pressure.

### 2.1. Linear Poroelasticity

[6] The rate of change in fluid mass,  $m$  (mass of fluid per unit bulk volume of porous material, with that volume being measured in the reference state from which we take strain as zero) is

$$\frac{m}{r_f} \approx \frac{a}{KB} B \frac{S_{kk}}{3} \quad (1)$$

where  $K$  is the drained bulk modulus of the porous material (i.e.,  $p = \text{const}$ ) and  $B$  is Skempton's coefficient. Under well-known conditions, both  $B$  and  $a$  may be expressed in terms of the respective bulk moduli of the solid and fluid components,  $K_s$  and  $K_f$ , and the porosity  $n$  (pore space per unit bulk volume in the reference state)

$$B \approx \frac{1}{1 - n} \frac{K - K_s}{K_s} \quad a \approx 1 - \frac{K}{K_s} \quad (2)$$

and  $a$  is Biot's coefficient. The  $a$  coefficient appears in the stress measure controlling strain rate in the elastic regime:  $\dot{\epsilon}_{ij} + a p \delta_{ij}$  [Biot, 1941; Nur and Byerlee, 1971; Rice and Cleary, 1976; Wang, 2000].

[7] The interpretation of Skempton's coefficient is that under undrained conditions ( $\dot{m} = 0$ ), the change in pore pressure is directly proportional to the change in total stress on an element:

$$p \approx B \frac{S_{kk}}{3} \quad (3)$$

For elastic-plastic response, the strain rate may be decomposed into elastic and plastic contributions:

$$D_{ij} = D_{ij}^e + D_{ij}^p \quad (4)$$

The linear poroelastic constitutive relations give the elastic strain rate of the bulk material,  $D_{ij}^e$ , as a function of the rates of total stress on the bulk material,  $S_{ij}$ , and pore pressure,  $p$ :

$$D_{ij}^e = \frac{1}{2G} S_{ij} + \frac{d_{ij}}{3K} \frac{S_{kk}}{3} + \alpha p \quad (5)$$

where  $G$  is the shear modulus and  $s_{ij} = S_{ij} - d_{ij}S_{kk}/3$  is the deviatoric stress tensor.

[8] For drained behavior  $p = 0$ , (5) simplifies to

$$D_{ij}^e = \frac{1}{2G} S_{ij} + \frac{d_{ij}}{3K} \frac{S_{kk}}{3} \quad (6)$$

For undrained behavior ( $\bar{m} = 0$ ), using (3) simplifies (5) to

$$D_{ij}^e = \frac{1}{2G} S_{ij} + \frac{d_{ij}}{3K_u} \frac{S_{kk}}{3} \quad (7)$$

where  $K_u$  is the undrained bulk modulus [Rice and Cleary, 1976]:

$$K_u = \frac{K}{1 - \alpha B} \quad (8)$$

Given the short time of stressing associated with rupture propagation, we can reasonably expect undrained deformation of the off-fault material for large enough lengths. The propagation speed of the rupture is generally of the order of the shear wave speed  $C_s$  and the region about which significant deformation occurs is expected [Poliakov et al., 2002; Rice et al., 2005; Templeton and Rice, 2008] to be on the order of the slip-weakening scale length  $R_o$  (see captions of Figures 1 and 3), argued from seismic constraints to be of the order of a few tens of meters at midseismogenic zone depths [Rice et al., 2005]. Rice [2006] has shown on the basis of lab data for intact ultracataclastic gouge that such material is expected to have a hydraulic diffusivity,  $a_{hy}$ , of order of  $10^{-6} \text{ m}^2/\text{s}$  at midseismogenic depths. The hydraulic diffusivity is  $a_{hy} = k/(h_f b_{st})$  where  $k$  is the permeability (the component of greatest uncertainty),  $h_f$  is the fluid viscosity, and  $b_{st}$  is a storage coefficient. Even allowing for up to  $10^6$  more permeability for other, less finely grained, materials of the damage zone, would allow for diffusivities of order  $10^{-6}$  to  $1 \text{ m}^2/\text{s}$ . To consider deformation as effectively undrained, we compare the diffusive length associated with the time  $R_o/C_s$  of coseismic stressing to the expected length scale of deformation

$$\frac{p}{a_{hy} R_o = C_s} \approx \frac{r}{R_o C_s} \quad (9)$$

which is  $\ll 1$  for the estimated values of  $R_o$  and  $a_{hy}$  and the shear wave speed being of order of  $\text{km/s}$ . Therefore, we can reasonably expect undrained deformation except down to short diffusive length scales of order of a few millimeters to centimeters.

## 2.2. Poroelastoplasticity

[9] Using results from Rice [1977] and Rudnicki [1984b, 2000] (see also Appendices A and B), we extend the equations governing plastic increments in strain introduced in part 1 to the fluid-saturated state.

[10] The first result is that plastic dilatational strain appears only as a plastic increment in pore space and consequently, (1) may be written as

$$\bar{m} = r_f \frac{a}{KB} + p + B \frac{S_{kk}}{3} + r_f D_{kk}^p \quad (10)$$

The additional result of Rice [1977] is that the appropriate effective stress measure for evaluating plastic strain increments is the Terzaghi effective stress

$$s_{ij}^0 = S_{ij} - p d_{ij} \quad (11)$$

Consequently, using the flow rule and pressure-dependent yield criterion introduced in part 1, we find that

$$D_{ij}^p = \frac{1}{h} \frac{S_{ij}}{2t} + d_{ij} \frac{b}{3} \frac{S_{kl}}{2t} + d_{kl} \frac{m}{3} \frac{\partial s_{kl}}{\partial s_{kl}} + p d_{kl} \quad (12)$$

where  $t$ , the scalar measure of shear stress, is the second invariant of  $s_{ij}$

$$t = \frac{r}{2} S_{ij} S_{ij} \quad (13)$$

and where  $h$  is a measure of material hardening,  $m$  is the internal friction parameter in the Drucker-Prager yield criterion (Appendix B), and  $b$  is the measure of inelastic dilatancy taken to be the ratio of  $D_{kk}^p$  to the equivalent plastic shear strain,  $g^{pl}$ , defined in Appendix B. For drained behavior (i.e.,  $p = 0$ ), the plastic strain increments are readily seen to be

$$D_{ij}^p = \frac{1}{h} \frac{S_{ij}}{2t} + d_{ij} \frac{b}{3} \frac{S_{kl}}{2t} + d_{kl} \frac{m}{3} S_{kl} \quad (14)$$

as used in part 1.

[11] For undrained behavior (i.e.,  $\bar{m} = 0$ ), the plastic strain increment expression has been shown to be identical in form to that for drained increments, but with replacement of the drained parameters  $h$ ,  $m$ , and  $b$  with new effective undrained parameters  $h_u$ ,  $m_u$ ,  $b_u$ . This undrained inelastic behavior was first noted in the analysis of simple shear deformation to affect the hardening term ( $h_u > h$  is characterized as “dilatant hardening”) [Rice, 1975a; Rice and Rudnicki, 1979]. Later work [Rudnicki, 1984b, 2000; Benallal and Comi, 2002, 2003] investigated the general constitutive response of equations (5), (10), and (12) with  $\bar{m} = 0$  and

found that in all such (undrained) deformations with plasticity the total strain rate is

$$D_{ij} \approx D_{ij}^e \approx D_{ij}^p \approx \frac{s_{ij}}{2G} \approx \frac{d_{ij}}{3K_u} \approx \frac{s_{kk}}{3} \approx \frac{1}{h_u} \approx \frac{s_{ij}}{2t} \approx \frac{b_u}{3} \approx \frac{s_{kl}}{2t} \approx \frac{m_u}{3} \approx s_{kl} \quad (15)$$

where  $h_u$ ,  $b_u$ , and  $m_u$  are effective undrained plastic material parameters, defined as

$$h_u \approx h \approx \frac{mbKB}{a} \quad (16)$$

$$b_u \approx b \approx Bb \quad (17)$$

$$m_u \approx m \approx Bm \quad (18)$$

If we normalize strain by  $t_p/2G$  and stress by  $t_p$  in equations (15)–(18), noting that  $K/G = 2(1+n)/[3(1-2n)]$  and similarly for  $K_u/G$  replacing  $n$  with  $n_u$ , the undrained Poisson ratio, we find that for a given  $s_{ij}^0/t_p$ , the relevant parameters describing increments in strain are:  $n_u$ ,  $h_u/G$ ,  $m_u$ , and  $b_u$ , or equivalently in terms of more primitive drained and poroelastic properties,  $n$ ,  $h/G$ ,  $m$ ,  $b$ ,  $a$ , and  $B$ .

[12] As part of deriving equations (15)–(18) the undrained change in pore pressure in a poroelastoplastic material with plastic dilatancy can be decomposed into a regular elastic undrained response and an additional term due to plastic dilatancy,

$$p \approx B \frac{s_{kk}}{3} \approx b \frac{KB}{a} \approx \frac{t_p m}{h} \approx \frac{Bb s_{kk}}{a} \quad (19)$$

In addition to these undrained parameters, when considering the yield function in the undrained state (see Templeton and Rice [2008] for a full introduction)

$$t \approx m \frac{s_{kk}}{3} \approx b \approx 0 \quad (20)$$

an effective cohesion,  $b_u$ , must be included to fully represent undrained behavior

$$b_u \approx b \approx Bm \frac{s_{kk}^0}{3} \quad (21)$$

where  $s_{kk}^0$  is the trace of the initial effective stress. That is, the stresses  $s_{ij}$ , defined as the initial effective stress  $s_{ij}^0$  plus the change  $Ds_{ij}$  in total stress associated with the rapid undrained deformation,  $s_{ij} = s_{ij}^0 + Ds_{ij}$ , will, at the onset of plastic response, satisfy

$$t \approx m_u \frac{s_{kk}}{3} \approx b_u \approx 0 \quad (22)$$

Figure 2 shows a drained and the corresponding undrained yield function. Note the material becomes easier to yield during undrained deformation when the mean normal stress is more compressive than the initial value. Similarly, the

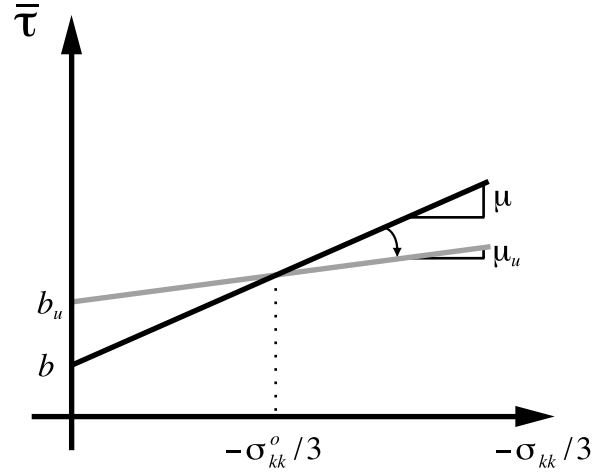


Figure 2. Illustration of the effective undrained cohesion,  $b_u$ , and internal friction coefficient,  $m_u$ , for a given initial effective stress state,  $s_{ij}^0$ , drained cohesion,  $b$ , and drained internal friction,  $m$ . Here  $s_{kk} = s_{kk}^0 + Ds_{kk}$ , where  $Ds_{kk}$  is the total stress change that occurs under undrained conditions; and here  $t$  is based on  $s_{ij}$ , where  $s_{ij} = s_{ij}^0 + Ds_{ij}$ , where  $s_{ij}^0$  is independent of initial pore pressure.

material becomes stronger when the mean normal stress is more tensile than the initial value.

[13] The derivation of the undrained material parameters is available in Appendix B. Clearly, the transformation of parameters embodied in equations (8), (16)–(18), and (22), transforms the undrained elastic-plastic problem into one of precisely the same form as the solutions of part 1 that neglected changes of pore pressure. Any solution given in that part 1 may be reinterpreted as an undrained solution for a material of different parameters, and conversely for the solutions given in this part.

### 2.3. Slip-Weakening Friction

[14] We approximate the shear strength of the fault during rupture as a normal stress-dependent Coulomb friction law with a peak strength  $t_p$  that degrades with slip  $Du$  to a residual strength,  $t_r$  over a characteristic length scale  $D_c$  (Figure 3b) [Ida, 1972; Palmer and Rice, 1973]:

$$t \approx \frac{t_p}{t_r} \left( t_r - t_r \frac{Du}{D_c} \right); \quad \frac{Du}{D_c} > \frac{D_c}{D_c} \quad (23)$$

where we take the peak and residual strengths to be the product of the fault-normal effective stress,  $s_n^0 = s_n + p_f$ , and peak and residual friction coefficients  $f_p$  and  $f_r$ , respectively, where  $p_f$  is the pore fluid pressure on the fault plane. A measure of the initial fault shear stress relative to the fault peak and residual strengths is the seismic  $S$  ratio:

$$S \approx \frac{t_p}{s_{xy}^0} \frac{s_{xy}^0}{t_r} \quad (24)$$

For the elastic case, in which there are no contrasts in hydraulic diffusivities and poroelastic properties across the fault, there is no change in the on-fault pore pressure due to the antisymmetry of the change in mean-normal pressure on

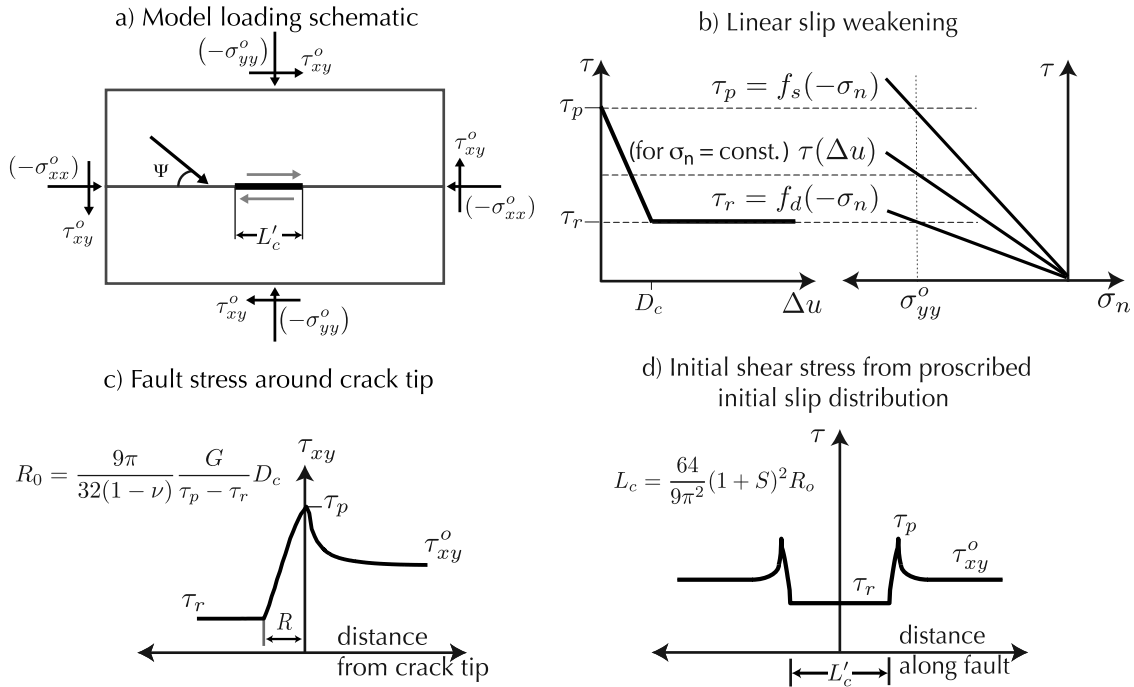


Figure 3. (a) A 2-D model geometry with initial stresses resulting in an angle of most compressive stress to the fault,  $\Psi$ . The right-lateral rupture is nucleated in the center of the fault along length  $L_c^0$ . (b) Linear slip-weakening friction model used to describe the degradation of the shear strength of the fault from a peak to a residual strength as a function of slip along the fault. (c) Example stress distribution around crack tip during propagation;  $R_0$  is the size of  $R$  in the limit of low rupture speed and large seismic  $S$  ratio,  $G$  is shear modulus. (d) Fault shear stresses resulting from proscribed initial slip distribution over length  $L_c^0$  slightly greater than static nucleation length estimate  $L_c$ .

each side of the fault. However, for that elastic case, where there is a contrast of properties across the fault, the pore pressure change on the fault itself would depend on the respective permeabilities and storage coefficients on the compressional and extensional side of the fault [Rudnicki and Rice, 2006; Dunham and Rice, 2008]. As an example, a rupture through a fault with more permeable material on the compressional side of the fault than on the extensional side would induce a net pore pressure increase on the fault, favoring further instability and rupture. For a dynamic rupture with crack-like response, this effect can either compete against or enhance the effect of an elastic property contrast.

[15] For our first investigations as reported here, for simplicity we neglect change in pore fluid pressure on the fault. Their full inclusion, left to future study, requires an alteration from standard finite element analysis for rupture dynamics. As already clear from the elastic analyses cited, whether the fault pore pressure  $p_f$  increases or decreases will be sensitive to material properties, especially permeability, on the few millimeters to centimeters scale within the damage zones on the two sides of the slip surface. As shown in part 1, plastic deformation occurs asymmetrically about and near the fault and consequently introduces a deviation from pure antisymmetry in the fault-parallel stress changes and in the amount of plastic dilatation. We would therefore expect some change in pore pressure on the fault, even for similar poroelastic properties and permeabilities

across the fault; if dilatancy had the dominant effect on pore pressure change, we may expect a stabilization on the fault through an increase in the effective fault-normal stress. While changes to rupture acceleration will change the development over distance of the extent and magnitude of stress around the crack tip (being functions of rupture velocity), we focus here on the effect of saturated off-fault material on plastic deformation patterns in comparison with those patterns found in the dry counterparts, as in part 1. Therefore we neglect in this study the effects of pore pressure increases or decreases on the slip-weakening response of the fault. Such slip weakening, as conventionally assumed, may in fact be a proxy for much more significant but highly localized pore pressure changes along the fault due to thermal pressurization [Sibson, 1973; Lachenbruch, 1980; Mase and Smith, 1987; Andrews, 2002; Noda and Shimamoto, 2005; Rice, 2006; Rempel and Rice, 2006; Suzuki and Yamashita, 2006; Bizzarri and Cocco, 2006].

[16] For a stationary crack, this fault constitutive relation results in a length scale,  $R_0$ , over which the strength drops from peak to residual behind the crack tip (Figure 3c), given approximately by [Palmer and Rice, 1973]

$$R_0 \approx \frac{9\pi}{16\delta 1} \frac{G}{t_p} \frac{G}{t_r^2} \quad \delta 25b$$

where  $G$  is the fracture energy ( $G = (t_p - t_r)D_c/2$  for linear slip weakening) and  $n$  is the Poisson ratio. Rice et al. [2005] estimated  $R_0$  to range from approximately 1 m to 40 m at midseismogenic crustal depth based on estimates of  $G$  using seismic slip inversion results of Heaton, [1990] and an assumed fault strength drop  $t_p - t_d$  based on  $f_s = 0.6$  and much smaller  $f_d$ .

### 3. Numerical Procedure

#### 3.1. Implementation

[17] As outlined in part 1, we use the finite element method, in the form of ABAQUS/Explicit, [ABAQUS, Inc., 2005] to model dynamic mode II shear rupture propagation in elastic-plastic material. The rupture direction and slip direction coincide and are in the  $x$  direction (Figure 3a). The fault plane is parallel to the intermediate principal stress direction of the tectonic prestress,  $s_{ij}^0$ . A 2-D rectangular mesh composed of linear four-noded linear reduced integration plane strain elements and containing a horizontal fault is used to model shear rupture propagation along the fault and the resulting off-fault stresses and deformation.

[18] Initial effective stress in the material surrounding the fault is  $s_{ij}^0$ , taken here for the reasons explained to be the effective prestress,  $s_{ij}^{0, \text{total}} + p^0 d_{ij}$ , which is based on the total prestress and  $p^0$  as an ambient pore pressure prevailing at midseismogenic depth. We compare ruptures in dry material to those in saturated material at the same initial effective stress. The angle of the most compressive effective stress to the fault is  $Y$  (Figure 3a). The initial effective stress state is uniform and the out of plane principal stress is  $s_{zz}^0 = (s_{xx}^0 + s_{yy}^0)/2$ , meaning that  $s_{zz}^0 = 0$ , so the Mohr-Coulomb and Drucker-Prager failure criteria initially coincide (see part 1). The deformation of the off-fault material in response to stress change  $Ds_{ij}$  follows the undrained constitutive law outlined in section 2, with  $s_{ij}$  identified as  $s_{ij}^0 + Ds_{ij}$ .

[19] All stresses in the analyses are nondimensionalized by the initial fault-normal effective stress,  $s_{yy}^0$ , and lengths are nondimensionalized by  $R_0$ , the length of the static, low stress drop, slip-weakening zone, as given in (25). The element spacing  $Dx$  is chosen so that the static slip-weakening zone is well resolved, with  $Dx = R_0/20$ .

[20] A mode II shear rupture is nucleated on the fault by altering the initial shear stress distribution along a portion of the fault of length  $L_c^0$  in Figure 3a. The initial shear stress distribution prescribed along the nucleation zone is produced using linear slip weakening for an initial slip distribution like in the work by Kame et al. [2003]. The length of the nucleation zone,  $L_c^0$ , is slightly greater than the critical nucleation length,

$$L_c \approx \frac{16}{3p} \frac{GG}{s_{xy}^0 t_r} \approx \frac{64}{9p^2} \frac{t_p - t_r}{s_{xy}^0 t_r} R_0 \quad (26b)$$

at which a static crack becomes unstable for the large  $S$  limit coinciding with singular elastic crack mechanics with small-scale yielding. The initial alteration in shear stress along length  $L_c^0$  results in a stress concentration slightly larger than the peak strength at the tips of the static nucleation zone. This initiates a dynamic rupture at both ends of the

nucleation zone at the start of the simulation to produce a bilateral right-lateral shear rupture. Along the predefined fault, a split node contact procedure is used to prescribe the shear strength, whose evolution follows (23). Details of the implementation of the split node procedure are given in the Appendix B of part 1.

[21] The entire mesh is surrounded by absorbing elements to minimize reflections from the boundaries. These elements introduce normal and shear tractions on the boundary of the finite element mesh that are proportional to the normal and shear components of velocity at the boundary, with damping constants chosen as the wave impedance factors to minimize reflections of dilational and shear wave energy. These elements perform best when the incident waves arrive perpendicular to the absorbing elements. Forces are applied between the boundary of the plane strain elements and the infinite elements consistent with the prescribed initial stress state.

#### 3.2. Parameter Selection

[22] Data for intact ultracataclasite fault gouge, summarized by Rice [2006], Table 1, as well as corrections for increased damage by an order of magnitude increase in permeability and a doubling of drained compressibility give  $B$  values ranging from 0.6–0.9 and  $a$  values ranging from 0.65–0.96. Rice and Cleary [1976] provide data in their Table 1 for a variety of sandstones and granites. After correcting the fluid compressibility to a more representative value for midseismogenic depth conditions, the  $B$  values range from 0.4–0.8 and values of  $a$  are between 0.24 and 0.78. In our simulations, we use  $n = 0.25$ ,  $a = 0.45$  and values of  $B$  ranging from 0.5 to 0.9. The undrained Poisson ratios corresponding to values of the Skempton coefficient  $B = 0.5, 0.7, 0.9$  are, respectively,  $n_u = 0.30, 0.32, 0.34$ . In results shown here we treat the drained response as ideally plastic, taking  $h/G = 0$ . Values for the inelastic internal friction and dilatancy coefficients  $m$  and  $b$  are given by Rudnicki and Rice [1975] on the basis of rock triaxial experiments conducted by Brace et al. [1966]. The values for  $m$  and  $b$  of Westerley granite, over a range of confining pressures, are respectively 0.4–0.9 and 0.2–0.4. Here we use an intermediate value for internal friction ( $m = 0.6$ , consistent with  $\tan f = 0.75$  in the Mohr-Coulomb criterion, using  $m = \sin f$ ) and when we consider inelastic dilatancy, we examine the range of values,  $b = 0$ –0.4. In section 4.1, we compare the effects of varying the Skempton coefficient and plastic dilation.

[23] We define the initial effective stress state using the angle the most compressive initial effective stress makes to the fault,  $Y$ , the fault frictional parameters,  $f_s$  and  $f_d$ , and the ratio  $S$  relating the initial fault shear stress to the peak and residual fault strength. Additionally, we verify that the initial stress state does not violate our Drucker-Prager yield criterion. We define a measure of closeness to failure (see part 1 for additional discussion) as

$$CF \approx \frac{t}{ms_{kk}^0 - 3pb} \quad (27b)$$

If  $CF > 1$  the initial state of stress violates the yield criterion. Note, the definition of  $b_u$  is such that using the undrained



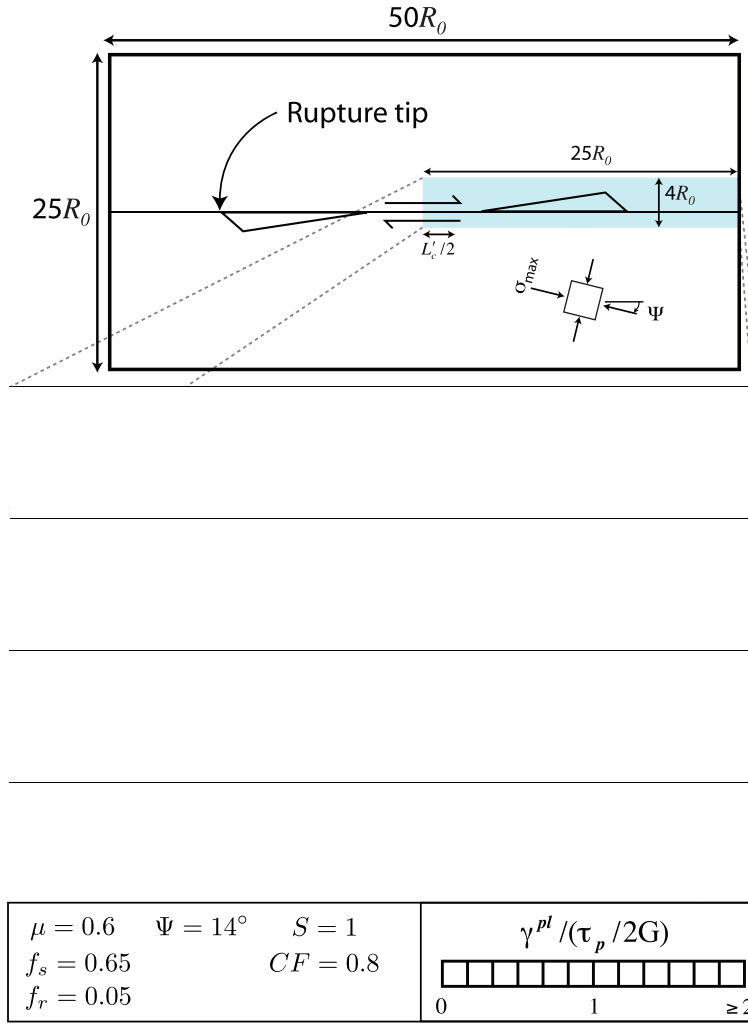


Figure 4. Contour plots of  $\gamma^{pl}/(\tau_p/2G)$  as a function of distance from the fault for  $S = 1$ , for  $\Psi = 14^\circ$ , fixed on- and off-fault strength parameters ( $f_s = 0.65$ ,  $f_d = 0.05$ ;  $m = 0.6$  ( $\tan f = 0.75$ )), fixed closeness of the initial stress state to off-fault failure ( $CF = 0.8$ ), and no plastic dilatation. We consider a case in which pore pressure changes are neglected ( $Dp = 0$ ) and undrained cases for which an increase of the Skempton coefficient ( $B = 0.5, 0.7, 0.9$ ) illustrates the role of undrained pore pressure generation in increasing the extent of inelastic deformation.

material parameters  $m_u$  and  $b_u$  in place of the drained parameters would not change  $CF$ .

## 4. Results and Discussion

### 4.1. Effect of Undrained Pore Pressure Generation on Extent of Inelastic Deformation

[24] Initially considering the off-fault material to be poroelastoplastic with no plastic dilatation, we find that changes in pore pressure significantly increase or decrease the amount of off-fault inelastic deformation. Assuming zero plastic dilatation, the only source of changing pore pressure is from the elastic part of the response. Therefore, the pore pressure response to stressing under undrained conditions is then described by values of the Skempton coefficient,  $B$ . Since the changes in pore pressure are proportional to changes in mean normal stress on the bulk material, one may expect during rupture propagation that pore pressure increases on the compressional side of the

fault and pore pressure decreases on the extensional side. These increases and decreases in pressure decrease or increase, respectively, the effective normal compressive stress, and bring the material closer or further from failure.

[25] In Figure 4, we plot the distribution of inelastic deformation (in terms of the equivalent plastic shear strain  $\gamma^{pl}$  defined as the time integral of  $\dot{\gamma}^{pl}$ , defined in Appendix B) about one side of a bilateral rupture on a right-lateral fault. Here we consider a single, shallow angle ( $14^\circ$ ) of the initial most compressive stress, and the initial effective stress state is further characterized by a seismic  $S$  ratio value of 1.0, with fixed fault frictional parameters  $f_s = 0.65$ ,  $f_d = 0.05$ , and off-fault material friction parameter  $m = 0.6$ . We consider the drained response (i.e., neglecting changes in  $p$ ) and undrained response, for three cases in which we vary the value of the Skempton coefficient ( $B = 0.5, 0.7, 0.9$ ). When pore pressure changes are neglected or absent, the inelastic deformation occurs on both the compressional and extensional side of the fault. Considering saturated off-

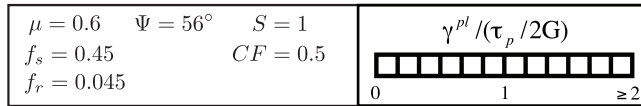


Figure 5. Contour plots of  $\gamma^{pl}/(\tau_p/2G)$  as a function of distance from the fault for  $S = 1, Y = 56$ , fixed on- and off-fault strength parameters ( $f_s = 0.45$ ,  $f_d = 0.045$ ;  $m = 0.6$ ), fixed closeness of the initial stress state to off-fault failure ( $CF = 0.5$ ), and no plastic dilation. We consider a case in which pore pressure changes are neglected ( $\Delta p = 0$ ) and undrained cases for which an increase of the Skempton coefficient ( $B = 0.5, 0.7, 0.9$ ). As a contrast to a shallower angle ( $Y = 14$ , Figure 4), the drained response exhibits deformation on the extensional side of the fault. Here the undrained cases ( $B = 0.5, 0.7, 0.9$ ) show a decrease in inelastic deformation.

fault material (and momentarily neglecting inelastic dilatation), we find that the extensional side is completely strengthened against inelastic deformation and the compressional side is weakened by respective coseismic pore pressure decreases and increases. The compressional side

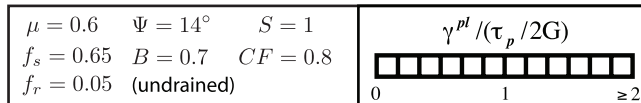


Figure 6. Contours of  $\gamma^{pl}/(\tau_p/2G)$  as a function of distance from the fault, with all parameters the same as in Figure 4, except here we consider the effects of inelastic dilatancy on the undrained response. For the case of Figure 4 in which  $B = 0.7$  (repeated at top here), increasing plastic dilatancy ( $b = 0, 0.2, 0.4$ ) has significant effect on reducing the extent of inelastic deformation.

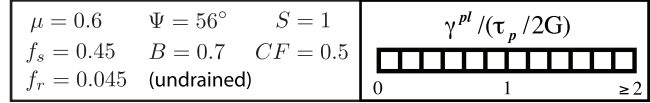


Figure 7. Contours of  $\gamma^{pl}/(\tau_p/2G)$  as a function of distance from the fault, with all parameters the same as in Figure 5, except here we consider the effects of inelastic dilatancy on the undrained response. For the case of Figure 4 in which  $B = 0.7$  (repeated at top here), introducing plastic dilatancy serves to reduce the extent plasticity but does not have as significant effect as in Figure 6.

is further weakened, as expected, with increases of the Skempton coefficient.

[26] In Figure 5, we plot the distribution of inelastic deformation for a steeper  $Y$  ( $56^\circ$ ), holding the same values of  $f_s$ ,  $f_d$ ,  $m$ , and varying over the same values of  $B$  as in Figure 4. Unlike in the case for a shallower  $Y$ , here we find that to the extent the fault has ruptured, for a steeper  $Y$  and the absence of pore pressure changes, the inelastic deformation occurs on the extensional side of the fault. As expected, increasing values of  $B$  leads to an increasing reduction in the extent of the plastically deforming region.

[27] In Figure 6, we consider the effect of undrained response with inelastic dilatancy and plot the equivalent

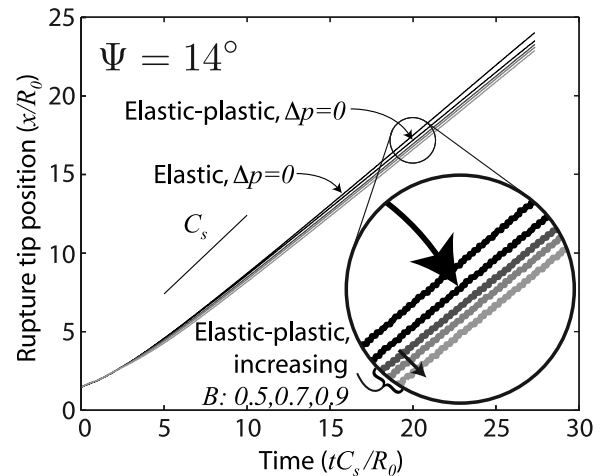


Figure 8. Plot of normalized rupture tip position versus normalized time for drained and undrained  $Y = 14$  cases of Figure 4 (i.e., without inelastic dilatancy). Here  $C_s$  is the shear wave speed. The increasing extent of inelastic deformation from drained to undrained responses is reflected in the slight delay for the rupture tip to reach a particular distance of the fault.



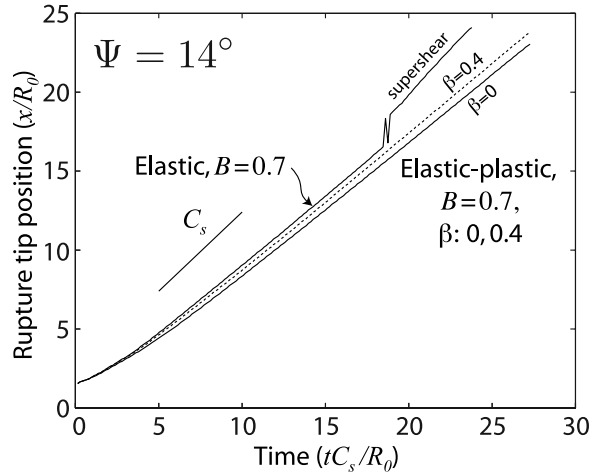


Figure 9. Plot of normalized rupture tip position versus normalized time for undrained  $\Psi = 14^\circ$  cases of Figure 6 with and without dilatancy. Here, the decreasing extent of inelastic deformation with increasing dilatancy is reflected in the slight decrease in time for the rupture tip to reach a particular distance of the fault. In addition to the cases presented in Figure 6, we also consider a case of rupture in an undrained elastic medium. In Figure 8 we considered a similar elastic case neglecting pore pressure changes. Here we find that under undrained conditions, the rupture transitions to supershear.

plastic shear strain about one side of a bilateral rupture on a right-lateral fault. Here we again consider a single, shallow angle ( $14^\circ$ ) of the initial most compressive stress, with the same initial stress state and material parameters, except here we allow inelastic dilatancy ( $b = 0.2-0.4$ ) for the case of Figure 4 that formerly had no such dilatancy and  $B = 0.7$ . Here we might expect that the pore pressure reduction due to plastic dilatancy would work against the pore pressure increase on the compressional side of the fault due to the elastic response. In comparison with the case of no inelastic dilatancy, we find that there is a significant decrease in magnitude and extent of inelastic deformation left behind by the rupture front. Additionally, we see an increase of

inelastic deformation occurring at acute angles ahead of the rupture front. For a large value of  $b$ , 0.4, we find that the increase in plastic deformation due to pore pressure increases is reduced by plastic dilatancy to the point of reducing the extent of deformation approximately to the original, drained ( $D_p = 0$ ) calculation in Figure 4.

[28] In Figure 7, for the steep ( $56^\circ$ ) prestress angle, we plot the distribution of inelastic deformation holding the same values of  $f_s$ ,  $f_d$ ,  $m$ , and examine the effect of inelastic dilatancy as in Figure 6. Here, pore pressure reductions from dilatancy act in conjunction with those reductions due to the poroelastic material response to reduce the extent and magnitude of the inelastic deformation. The further reduction from the introduction of inelastic dilatancy is slight relative to the reductions due to changes of pressure from solely poroelastic behavior.

[29] With the additional allowance for plastic dilatancy (i.e., the creation of pore space through inelastic deformation), we find that the overall effect is to reduce inelastic deformation (note that the equivalent plastic shear strain, to which the dilation is proportional, is small and of order  $t_p/G$  in the off-fault region). The creation of additional pore space due to plastic dilatation under undrained conditions creates a decrease in pore pressure, irrespective of whether a point is considered on the extensional or compressional side of the fault. Thus, plastic dilatation serves as a mechanism to increase the effective stress and reduce initiated inelastic deformation. Equivalently, we may say that the material is dilatantly hardened.

#### 4.2. Effect of Pore Pressure-Induced Changes in Inelastic Deformation on Rupture Propagation

[30] The reduction or increase in the amount of off-fault plastic work being done as the rupture passes affects the rupture propagation [Andrews, 2005]. In the cases presented in Figures 4 and 5, where undrained pore pressure generation controlled by the material Skempton coefficient prohibits or encourages failure, the varying amount of plastic work is readily evident by the changing extent and magnitude of plastic deformation. Figure 8 plots the position of the rupture front versus time for the cases presented in Figure 4 and for the case of rupture in an elastic material not

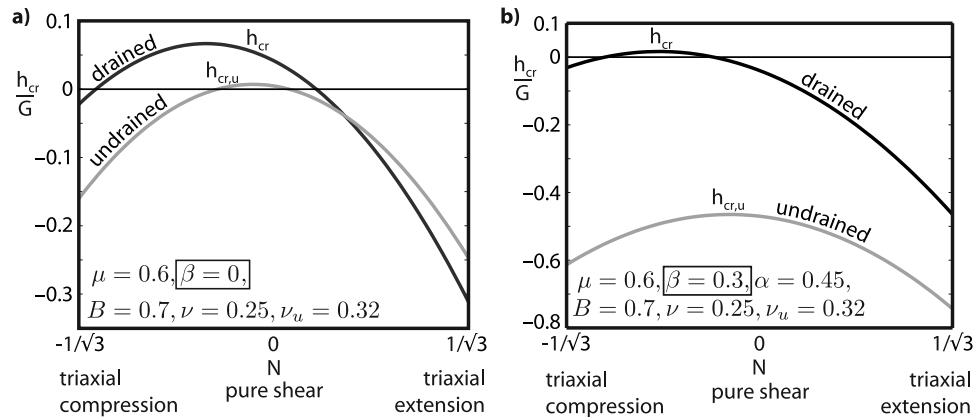


Figure 10. Plots of the normalized critical value of hardening  $h_{cr}$ , at which localization is expected to occur for static loading, versus the stress state parameter  $N$ . No localization of deformation is expected if  $h < h_{cr}$ . (a) We neglect effects of inelastic dilatancy ( $b = 0$ ). (b) We consider a dilatancy  $b = 0.3$  and hold all other parameters fixed. Note the effect of dilatant hardening in the reduction of  $h_{cr,u}$ .

including changes in pore pressure. Here, the net effect of the undrained response, not considering inelastic dilation, is an increase in the extent and magnitude of inelastic deformation. Consequently, the rupture propagates slightly more slowly with increasing extent. For the cases of Figure 6 in which we evaluate inelastic dilatancy during the rupture under undrained conditions, the net effect is a reduction in the extent in deformation. Here in Figure 9 the result is a speeding up of rupture propagation that approaches the undrained poroelastic solution as the extent is decreased. Additionally, there is found a suppression (or delay) of the transition to supershear in some cases evaluated where plasticity was incorporated in part 1 [Templeton and Rice, 2008].

#### 4.3. Role of Undrained Conditions and Plastic Dilatancy in the Elimination of Plastic Localization

[31] Part 1 has shown strain localization to be pervasive in the off-fault inelastic deformation during dynamic rupture when neglecting fluid saturation, at least for zero or even low positive values of hardening  $h$ . When fluid saturation is considered and the material is treated as undrained (i.e., no fluid diffusion occurs), these localization features apparently disappear (we have not done the extreme mesh refinements of part 1). On the basis of the work of Rudnicki and Rice [1975], it was shown in part 1 that the occurrence of these localization features stemming from the fault is essentially determined by the drained inelastic hardening modulus,  $h$ . Localization occurs when  $h$  falls below a critical hardening value,  $h_{cr}$ , which is determined by  $m$ ,  $b$ , and the normalized direction of the intermediate principal deviatoric stress,  $N$

$$\frac{h_{cr}}{G} \approx \frac{1}{90} \frac{1}{1+n} \frac{1}{n} \frac{1}{b} \frac{1}{m^2} \frac{1}{2} \frac{1}{N} \frac{1}{b} \frac{1}{m} \frac{1}{3} \quad (28)$$

where

$$N \approx \frac{1}{2} \frac{r}{s_{ij}} \quad (29)$$

This mode of localization (as opposed to compaction banding) is the only mode expected for low-porosity, dilating rocks, such as that considered in sections 4.1 and 4.2.

[32] We have shown that for undrained conditions, effective undrained parameters replace their drained counterparts. The consequence of this is that a critical undrained hardening may naively be calculated on the basis of (28). The result is that the critical hardening  $h_{cr}$ , now called  $h_{cr,u}$ , seems to be reduced drastically for most stress states (Figures 10a and 10b):

$$\frac{h_{cr,u}}{G} \approx \frac{1}{90} \frac{1}{1+n_u} \frac{1}{n_u} \frac{1}{b} \frac{1}{m^2} \frac{1}{2} \frac{1}{N} \frac{1}{b} \frac{1}{m} \frac{1}{3} \frac{K}{G} \frac{mbB}{a} \quad (30)$$

(the ratio  $K/G$  may be written  $2(1+n)/[3(1-2n)]$  where  $n$  is the Poisson ratio under drained conditions). Here for  $b = 0$ , as  $B \rightarrow 1$ ,  $h_{cr,u} \rightarrow 0$ , indicating that localization would not be as pervasive (or exist at all) for undrained cases, when the

drained  $h \rightarrow 0$ . Of course, this does not eliminate the possibility that the actual  $h$  may be large and negative (e.g., due to a loss of a cohesive strength component gained through cementation processes on the interseismic timescale), so that even undrained assumptions could make a negative  $h_{cr,u}$  larger than  $h$  and the localization issue would remain.

[33] However, consideration of  $h_{cr,u}$  must additionally be tempered by the fact that the undrained material is diffusively unstable [Rice, 1975a; Rudnicki, 1984a] when  $h < h_{cr}$  (the drained value of equation (28)), meaning that since fluid does diffuse over some sufficiently small length scale the material will tend toward drained behavior as time for the diffusion of fluid mass passes. Therefore, there is a competition between the timescale of stressing from the rupture tip and the timescale for fluid diffusion to a potential source of localized failure. For a high hydraulic diffusivity estimate for no longer intact granite of  $a_{hy} = 10^{-4} \text{ m}^2/\text{s}$  and a low estimation of expected localized failure thickness on the order of 100 mm, the characteristic timescale for diffusion is of the order of  $10^{-4} \text{ s}$ . If the region over which significant stressing occurs is on the order of  $R_0$ , thought to be a few tens of meters, and the rupture propagation is on the order of the shear wave speed, the corresponding timescale for stressing is  $10^{-2} \text{ s}$ . In such case this would be an issue requiring further examination, which we defer to future work. However, for an immature shear zone with a thickness of order 10 mm, the timescale for diffusion will increase with thickness and rise to the order of the stressing timescale. Therefore, for localized deformation on these larger length scales,  $h_{cr,u}$  may begin to be the representative hardening value, not considering the effects of significant softening.

#### 5. Conclusion

[34] Response of fluid-saturated materials is assumed to be effectively undrained on the short timescale of stress concentration near a passing rupture front along a fault. Poroelastic behavior and inelastic dilation then change the location and spatial extent of inelastic deformation patterns created by dynamic rupture. Undrained pressure changes due to the poroelastic response, which oppose isotropic changes in stress and are proportional to the Skempton coefficient  $B$ , strengthen the extensional side of the fault and weaken the compressional side against inelastic yielding. Inelastic dilatation, controlled by  $b$ , reduces pore pressure under undrained conditions and strengthens both sides. The undrained response can determine which side of the fault experiences inelastic deformation. For a case examined with a shallow prestress angle  $Y$ , inelastic deformation during rupture occurs on both sides of the fault when drained conditions are assumed. However, the undrained response can have the remarkable effect of completely strengthening the extensional side of the fault, leaving inelastic deformation to occur and increase in extent on the compressional side. For a steep angle  $Y$ , for which deformation occurs on the extensional side, the effect of undrained pore pressure change only serves to reduce the extent on the extensional side and are not sufficient to weaken the compressional side to the point of yielding. The changed pattern of inelastic deformation between drained and undrained cases only moderately affects the rupture propagation: for significant

increases in plastic deformation (e.g., for low  $Y$ ), the rupture in undrained material requires slightly more time to propagate to a comparable distance.

## Appendix A: Inelastic Constitutive Properties in the Deformation of Saturated Porous Media

[35] This section outlines and gives in somewhat greater detail the arguments presented in an extended abstract [Rice, 1977], drawing on the constitutive methodology of Rice [1971, 1975b], and providing some constraints on representing plastic strain and porosity changes in fluid-saturated geomaterials. The focus is on a representative volume of material that is undergoing locally heterogeneous inelastic deformation by frictional slip on contacting fissure surfaces and by open microcrack growth. The macroscopic average stress,  $s_{ij}$ , acting on the locally heterogeneous material can be regarded as determined by its macroscopic average strain,  $\epsilon_{ij}$ , its pore pressure,  $p$ , and the current state of locally heterogeneous inelastic slip on fissures and microcracking within the representative volume of material. The latter array of microscale variables is represented symbolically by  $H$ ; it would be impossible to describe them other than statistically, but the only properties that we need for  $H$  are these: when  $H$  is fixed (no slip on fissures, no crack growth) during an increment in  $s_{ij}$ ,  $\epsilon_{ij}$ , and  $p$ , the relation between those variables corresponds to normal poroelastic response. When there is an increment in local slip on fissures and/or microcrack growth, we understand there to be an increment in  $H$ , and the overall response is poroelastoplastic. Thus we can write

$$s_{ij} = s_{ij}(\epsilon_{kl}, p; H) \quad \text{A1b}$$

where the relation between the variables at fixed  $H$  describes a poroelastic relation.

[36] The strain energy  $u = u(\epsilon_{kl}, n, H)$  of the solid phase per unit reference state volume of the porous material then satisfies [e.g., Rice and Cleary, 1976], for fixed  $H$ ,

$$\frac{\partial u}{\partial \epsilon_{ij}} = s_{ij} \quad \frac{\partial u}{\partial p} = n \quad \text{A2b}$$

Letting  $y = y(s_{ij}, p, H) = s_{ij} \epsilon_{ij} + pn - u$ , it then follows that

$$\frac{\partial y}{\partial s_{ij}} = \epsilon_{ij} \quad \frac{\partial y}{\partial p} = n \quad \text{A3b}$$

where the derivatives are at fixed  $H$  and hence refer to elastic changes.

[37] We define plastic parts of the variations of functions like the above potential  $y$  as the change in the value of the potential due to variations in  $H$ , but with  $y$  evaluated for the same  $s_{ij}$  and  $p$

$$d^p y = y(s_{ij}, p; H + dH) - y(s_{ij}, p; H) \quad \text{A4b}$$

The plastic part [see Rice, 1971] of strain and porosity increments are  $d^p \epsilon_{ij} = \epsilon_{ij}(s_{ij}, p, H + dH) - \epsilon_{ij}(s_{ij}, p, H)$  and  $d^p n = n(s_{ij}, p, H + dH) - n(s_{ij}, p, H)$  and these satisfy

$$d^p \epsilon_{ij} = \frac{\partial d^p y}{\partial s_{ij}} \quad d^p n = \frac{\partial d^p y}{\partial p} \quad \text{A5b}$$

[38] We then let changes in states of microscopic solid inelastic deformation  $H$  and  $H + dH$  be characterized by incremental internal variables  $dx_k$  with corresponding work conjugate forces  $f_k(s_{ij}, p, H)$  such that the sum of their products when averaged over a representative macroscopic volume (where angle brackets represent the volume average of the quantity within the brackets) is

$$\langle f_k dx_k \rangle = d^p y \quad \text{A6b}$$

Consequently, from (A5) and (A6) the plastic variations of the strain and porosity are given by

$$d^p \epsilon_{ij} = \langle \frac{\partial f_k}{\partial s_{ij}} dx_k \rangle \quad d^p n = \langle \frac{\partial f_k}{\partial p} dx_k \rangle \quad \text{A7b}$$

[39] When considering a saturated, fissured rock mass or granular material, inelastic deformation may take the form of crack extension and frictional sliding along fissure surfaces. As introduced by Rice [1975b], the volume average representation of  $d^p \epsilon_{ij}$  in the case of microcrack extension within a representative volume  $V$  includes an integration over all crack front arcs ( $G_c$ ), with arc length  $s$ , of the local fracture energy release  $G_{loc}$  per unit advance of the crack area times the advance area  $da(s)ds$

$$\langle \frac{\partial f_k}{\partial s_{ij}} dx_k \rangle = \frac{1}{V} \int_{G_c} \frac{\partial G_{loc}(s_{ij}, p; H)}{\partial s_{ij}} da(s)ds \quad \text{A8b}$$

Similarly, in the case of frictional sliding along fissure surfaces  $S_f$ , which experience local slip increments  $d(Du)$  and over which local shear stress  $t$  acts in the slip direction, the volume average representation of  $d^p \epsilon_{ij}$  in (A7) can be expressed as

$$\langle \frac{\partial f_k}{\partial s_{ij}} dx_k \rangle = \frac{1}{V} \int_{S_f} \frac{\partial t(s_{ij}, p; H)}{\partial s_{ij}} dDu dS \quad \text{A9b}$$

[40] Now, we consider porous materials for which all pore spaces are in matter communication with the pore fluid and for which all of the solid phase has an identical isotropic elastic response to local increments in isotropic stress. The same special materials are considered for estimating some of the constants of poroelasticity [Nur and Byerlee, 1971; Rice and Cleary, 1976]. In those materials simultaneous macroscopic stress and pore pressure increments of the form

$$ds_{ij} = d_{ij} dP \quad dp = dP \quad \text{A10b}$$

result in a uniform, isotropic local stress increment  $ds_{ij}^{local} = d_{ij} dP$  at each microscale point of the solid phase. ( $s_{ij}^{local}$  is of course not equal to the macroscopic stress  $s_{ij}$ , but increments in  $ds_{ij}^{local}$ , when  $H$  is fixed, will be linearly proportional to increments  $ds_{ij}$  and  $dp$ , with local coefficients in that proportionality constrained by the requirement  $ds_{ij}^{local} = dP d_{ij}$  in the case of (A10).) Such isotropic changes in local stress do not alter local stress  $t$  or effective normal stress on fissures and, because they leave local crack tip singular stress fields unaffected, they do not

alter the local  $G$ . Thus such increments would not cause a change in the work conjugate forces  $f$  discussed above. Neither would they induce a further increment of plastic deformation, because they would not slip a fissure surface (if governed by normal concepts of effective stress) nor grow a crack if its growth is controlled by  $G$ .

[41] The increments  $ds_{ij}$  and  $dp$  considered are, of course, exactly those which cause no change in the macroscopic Terzaghi effective stress,

$$ds_{ij}^0 \approx \frac{1}{2} s_{ij} \approx \frac{1}{2} p d_{ij} \quad \partial A11b$$

and therefore their induction of no further plastic deformation means that the Terzaghi stress is the appropriate stress controlling macroscopic inelastic strain increments. An additional result of the force conjugate to microscopic inelastic deformation,  $f(s_{ij}, p, H)$ , remaining unaffected by stress increments in the form of (A10) is that

$$df \approx \frac{\partial f}{\partial s_{ij}} ds_{ij} \approx \frac{\partial f}{\partial p} dp \approx \frac{\partial f}{\partial s_{ij}} d_{ij} \approx \frac{\partial f}{\partial p} dp \approx 0 \quad \partial A12b$$

for an arbitrary increment  $dP$ . Hence, the term within the parentheses must be identically zero. Using (A12) and (A7), we find that

$$d^p_{kk} \approx \frac{1}{2} d^p_n \quad \partial A13b$$

i.e., plastic dilatancy is an inelastic increase in porosity.

## Appendix B: Derivation of Effective Material Parameters for Undrained Behavior

[42] When the stress state reaches a prescribed yield criterion, the material can deform plastically. The yield criterion is defined by the yield function  $F$ , such that  $F = 0$  when the material deforms plastically. The yield function for the Drucker-Prager criterion, as introduced in part 1 [Templeton and Rice, 2008] except here explicitly evaluated in terms of the Terzaghi effective stress, is

$$F \approx \frac{1}{2} \tau \approx \frac{1}{2} m \frac{S_{kk}}{3} \approx p \approx b \quad \partial B1b$$

Any hardening or softening of the material due to inelastic deformation is reflected by the movement of the yield surface in stress space. To ensure that the stress state continues to be on the yield surface during hardening, the stress state must satisfy  $\dot{F} = 0$

$$\tau \approx m \frac{S_{kk}}{3} \approx p \approx \frac{1}{2} b \approx m \frac{S_{kk}}{3} \approx p \quad \partial B2b$$

The terms  $b$  and  $m$  on the right-hand side of (B2) are the evolution of the yield criterion parameters. We define a hardening term  $h$  such that

$$b \approx m \frac{S_{kk}}{3} \approx p \approx \frac{1}{2} h g^{pl} \quad \partial B3b$$

where  $g^{pl}$  is the rate of the equivalent plastic shear strain ( $g^{pl}$ ) and, for conciseness, used to represent what was  $d^p g/dt$  in part 1:

$$g^{pl} \approx \frac{1}{2} \sqrt{\frac{1}{2} D_{ij}^p D_{ij}^p} \approx \frac{1}{2} \sqrt{\frac{1}{2} D_{ij}^p D_{ij}^p} \quad \partial B4b$$

Here if we take  $m$  to be constant, then  $\dot{m} = 0$  and the evolution of the yield surface results from changes in the cohesion  $b$  and is given by

$$\dot{b} \approx h g^{pl} \quad \partial B5b$$

From (B2) and (B3),

$$g^{pl} \approx \frac{1}{h} \tau \approx m \frac{S_{kk}}{3} \approx p \quad \partial B6b$$

and combining (19) and (B6),

$$g^{pl} \approx \frac{1}{h \approx m b K B = a} \tau \approx \frac{1}{B \approx m} \frac{S_{kk}}{3} \quad \partial B7b$$

This equation defines the effective internal friction parameter  $m_u$  and effective hardening parameter  $h_u$  as

$$m_u \approx \frac{1}{B \approx m} \quad h_u \approx h \approx \frac{m b K B}{a} \quad \partial B8b$$

[43] Undrained conditions introduce a new internal friction parameter,  $m_u$ . Under such conditions, changes in the deviatoric portion of the stress alone will not result in changes in pore pressure; therefore, the yield point above a given initial effective isotropic stress on a plot as in Figure 2 remains unchanged from yield point under drained conditions for the same initial effective isotropic stress. However, the introduction of  $m_u$  necessitates the introduction of a corresponding effective cohesion,  $b_u$ :

$$b_u \approx b \approx B m_s^0 = 3 \quad \partial B9b$$

[44] Thus, under undrained conditions the yield criterion  $F$  becomes

$$F \approx \tau \approx m_u \frac{S_{kk}}{3} \approx b_u \quad \partial B10b$$

Additionally, because the hardening  $h$  is replaced by an undrained value  $h_u$ , from equations (B2), (B7), (B9) and taking  $m$  to be constant,

$$b_u \approx h_u g^{pl} \quad \partial B11b$$

[45] Since plastic dilatancy changes (reduces) pore pressure, there is some feedback from plastic dilatation on the elastic strains. This is accounted for by expressing the elastic strain rate as the sum of the regular undrained elastic response  $D_{ij}^{R,e}$ , plus a correction to account for pore pressure changes due to plastic dilatancy  $D_{ij}^{P,e}$ :

$$D_{ij}^e \approx \frac{1}{2} D_{ij}^{R,e} \approx D_{ij}^{P,e} \quad \partial B12b$$



where the regular undrained elastic response is expressed in (7). For positive plastic dilatancy, the reduction in pore pressure will have the effect of reducing the elastic strain. This is accounted for in  $D_{ij}^{pe}$  by

$$D_{kk}^{pe} = \frac{a}{K} \frac{KB}{a} b \frac{t}{h} \frac{m\delta 1}{mbKB=a} \quad \delta B13b$$

where the term inside the brackets is the term in (19) giving the increment in pore pressure due to plastic dilatancy.

[46] Consequently, we define a contribution of plastic dilatancy to strain as a sum of changes in strain due to the plastic dilatancy itself and the feedback effect this dilatancy has on elastic strains:

$$D_{kk}^p \supset D_{kk}^{pe} \frac{1}{4} \delta 1 \quad Bb \frac{t}{h} \frac{m\delta 1}{mbKB=a} \quad \delta B14b$$

and we can thus define the effective plastic dilatancy as

$$b_u \frac{1}{4} \delta 1 \quad Bb \quad \delta B15b$$

[47] Acknowledgments. This study was supported by NSF-EAR award 0440145 and by the Southern California Earthquake Center (SCEC), funded by NSF Cooperative Agreement EAR-0106924 and USGS Cooperative Agreement 02HQAG0008 (this is SCEC contribution 1196), with additional funding from the Harvard University Center for the Environment in support of developing related concepts for landslides.

## References

- ABAQUS, Inc. (2005), ABAQUS theory manual, version 6.5, Providence, R. I.
- Andrews, D. J. (2002), A fault constitutive relation accounting for thermal pressurization of pore fluid, *J. Geophys. Res.*, 107(B12), 2363, doi:10.1029/2002JB001942.
- Andrews, D. J. (2005), Rupture dynamics with energy loss outside the slip zone, *J. Geophys. Res.*, 110, B01307, doi:10.1029/2004JB003191.
- Benallal, A., and C. Comi (2002), Material instabilities in inelastic saturated porous media under dynamic loadings, *Int. J. Solids Struct.*, 39, 3693–3716.
- Benallal, A., and C. Comi (2003), Perturbation growth and localization in fluid-saturated inelastic porous media under quasi-static loadings, *J. Mech. Phys. Solids*, 51, 851–899.
- Biot, M. A. (1941), General theory of three-dimensional consolidation, *J. Appl. Phys.*, 12, 155–164.
- Bizzarri, A., and M. Cocco (2006), A thermal pressurization model for the spontaneous dynamic rupture propagation on a three-dimensional fault: 1. Methodological approach, *J. Geophys. Res.*, 111, B05303, doi:10.1029/2005JB003862.
- Brace, W. F., B. W. Paulding, and C. Scholz (1966), Dilatancy in the fracture of crystalline rocks, *J. Geophys. Res.*, 71, 3939–3953.
- de Borst, R., J. Réthoré, and M. A. Abellan (2006), A numerical approach for arbitrary cracks in a fluid-saturated medium, *Arch. Appl. Mech.*, 75, 595–606.
- Dunham, E. M., and J. R. Rice (2008), Earthquake slip between dissimilar poroelastic materials, *J. Geophys. Res.*, doi:10.1029/2007JB005405, in press.
- Heaton, T. H. (1990), Evidence for and implications of self-healing pulses of slip in earthquake rupture, *Phys. Earth Planet. Inter.*, 64, 1–20.
- Ida, Y. (1972), Cohesive force across tip of a longitudinal-shear crack and Griffiths specific surface-energy, *J. Geophys. Res.*, 77, 3796–3805.
- Kame, N., J. R. Rice, and R. Dmowska (2003), Effects of pre-stress state and rupture velocity on dynamic fault branching, *J. Geophys. Res.*, 108(B5), 2265, doi:10.1029/2002JB002189.
- Lachenbruch, A. H. (1980), Frictional heating, fluid pressure, and the resistance to fault motion, *J. Geophys. Res.*, 85, 6097–6112.
- Mase, C. W., and L. Smith (1987), Effects of frictional heating on the thermal, hydrologic, and mechanical response of a fault, *J. Geophys. Res.*, 92, 6249–6272.
- Noda, H., and T. Shimamoto (2005), Thermal pressurization and slip-weakening distance of a fault: An example of the Hanaore fault, south-west Japan, *Bull. Seismol. Soc. Am.*, 95, 1224–1233.
- Nur, A., and J. D. Byerlee (1971), Exact effective stress law for elastic deformation of rock with fluids, *J. Geophys. Res.*, 76, 6414–6419.
- Palmer, A. C., and J. R. Rice (1973), Growth of slip surfaces in progressive failure of over-consolidated clay, *Proc. R. Soc. London, Ser. A.*, 332, 527–548.
- Poliakov, A. N. B., R. Dmowska, and J. R. Rice (2002), Dynamic shear rupture interactions with fault bends and off-axis secondary faulting, *J. Geophys. Res.*, 107(B11), 2295, doi:10.1029/2001JB000572.
- Rempel, A. W., and J. R. Rice (2006), Thermal pressurization and onset of melting in fault zones, *J. Geophys. Res.*, 111, B09314, doi:10.1029/2006JB004314.
- Réthoré, J., R. de Borst, and M. A. Abellan (2007), A discrete model for the dynamic propagation of shear bands in a fluid-saturated medium, *Int. J. Numer. Anal. Methods Geomech.*, 31, 347–370.
- Rice, J. R. (1971), Inelastic constitutive relations for solids—An internal-variable theory and its application to metal plasticity, *J. Mech. Phys. Solids*, 19, 433–455.
- Rice, J. R. (1975a), On the stability of dilatant hardening for saturated rock masses, *J. Geophys. Res.*, 80, 1531–1536.
- Rice, J. R. (1975b), Continuum mechanics and thermodynamics of plasticity in relation to microscale deformation mechanisms, in *Constitutive Equations in Plasticity*, edited by A. S. Argon, chapter 2, pp. 23–79, M. I. T. Press, Cambridge, Mass.
- Rice, J. R. (1977), Pore pressure effects in inelastic constitutive formulations for fissured rock masses, in *Advances in Civil Engineering Through Engineering Mechanics*, Proceedings of 2nd ASCE Engineering Mechanics Division Specialty Conference, N. C. Raleigh, 1977, pp. 295–297, Am. Soc. of Civ. Eng., New York.
- Rice, J. R. (2006), Heating and weakening of faults during earthquake slip, *J. Geophys. Res.*, 111, B05311, doi:10.1029/2005JB004006.
- Rice, J. R., and M. P. Cleary (1976), Some basic stress diffusion solutions for fluid-saturated elastic porous-media with compressible constituents, *Rev. Geophys.*, 14, 227–241.
- Rice, J. R., and J. W. Rudnicki (1979), Earthquake precursory effects due to pore fluid stabilization of a weakening fault zone, *J. Geophys. Res.*, 84, 2177–2193.
- Rice, J. R., C. G. Sammis, and R. Parsons (2005), Off-fault secondary failure induced by a dynamic slip pulse, *Bull. Seismol. Soc. Am.*, 95, 109–134.
- Rudnicki, J. W. (1984a), Effects of dilatant hardening on the development of concentrated shear deformation in fissured rock masses, *J. Geophys. Res.*, 89, 9259–9270.
- Rudnicki, J. W. (1984b), A class of elastic plastic constitutive laws for brittle rock, *J. Rheol.*, 28, 759–778.
- Rudnicki, J. W. (2000), Diffusive instabilities in dilating and compacting geomaterials, in *Multiscale Deformation and Fracture in Materials and Structures*, edited by T.-J. Chuang and J. W. Rudnicki, pp. 159–182, Kluwer Acad., New York.
- Rudnicki, J. W., and J. R. Rice (1975), Conditions for localization of deformation in pressure-sensitive dilatant materials, *J. Mech. Phys. Solids*, 23, 371–394.
- Rudnicki, J. W., and J. R. Rice (2006), Effective normal stress alteration due to pore pressure changes induced by dynamic slip propagation on a plane between dissimilar materials, *J. Geophys. Res.*, 111, B10308, doi:10.1029/2006JB004396.
- Sibson, R. H. (1973), Interactions between temperature and pore-fluid pressure during earthquake faulting and a mechanism for partial or total stress relief, *Nature Phys. Sci.*, 243, 66–68.
- Suzuki, T., and T. Yamashita (2006), Nonlinear thermoporoelastic effects on dynamic earthquake rupture, *J. Geophys. Res.*, 111, B03307, doi:10.1029/2005JB003810.
- Templeton, E. L., and J. R. Rice (2008), Off-fault plasticity and earthquake rupture dynamics: 1. Dry materials or neglect of fluid pressure changes, *J. Geophys. Res.*, 113, B09306, doi:10.1029/2007JB005529.
- Wang, H. F. (2000), *Theory of Linear Poroelasticity With Applications to Geomechanics and Hydrogeology*, Princeton Univ. Press, Princeton, N. J.
- J. R. Rice, E. L. Templeton, and R. C. Viesca, School of Engineering and Applied Sciences, Harvard University, 29 Oxford Street, Pierce Hall, Cambridge, MA 02138, USA. (rice@esag.harvard.edu; templet@fas.harvard.edu; viesca@seas.harvard.edu)